Clear Experimental Demonstration of Hole Gas Accumulation in Ge/Si Core–Shell Nanowires

Naoki Fukata,*,† Mingke Yu,† Wipakorn Jevasuwan,† Toshiaki Takei,† Yoshio Bando,† Wenzhuo Wu,‡ and Zhong Lin Wang†,‡

†International Center for Materials Nanoarchitectonics, National Institute for Materials Science, 1-1 Namiki, Tsukuba 305-0044, Japan and ‡School of Materials Science and Engineering, Georgia Institute of Technology, Atlanta, Georgia 30332-0245, United States

ABSTRACT Selective doping and band-offset in germanium (Ge)/silicon (Si) core–shell nanowire (NW) structures can realize a type of high electron mobility transistor structure in one-dimensional NWs by separating the carrier transport region from the impurity-doped region. Precise analysis, using Raman spectroscopy of the Ge optical phonon peak, can distinguish three effects: the phonon confinement effect, the stress effect due to the heterostructures, and the Fano effect. The Fano effect is the most important to demonstrate hole gas accumulation in Ge/Si core–shell NWs. Using these techniques, we obtained conclusive evidence of the hole gas accumulation in Ge/Si core–shell NWs. The control of hole gas concentration can be realized by changing the B-doping concentration in the Si shell.

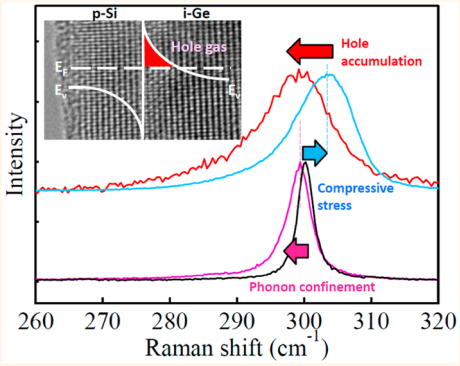

KEYWORDS: core–shell nanowires · doping · Raman scattering · Fano resonance

Considerable work has been done regarding one-dimensional semiconducting nanowires (NWs).[1–9] Silicon (Si) and germanium (Ge) NWs have attracted particular attention due to their compatibility with current Si complementary metal–oxide semiconductor (Si CMOS)-integrated circuit technology and their better scalability. These NWs have potential for use in the channel, source, and drain regions of MOS field-effect transistors (FETs). However, the problem of retardation of carrier mobility caused by impurity scattering must be solved if impurity atoms are doped into the channel region. Core–shell NWs using Si and Ge appear to have major potential for suppression of impurity scattering.[10–24] A radial heterojunction design separates the carrier transport pathway from the impurity-doped regions. This structure is similar to that in high electron mobility transistors.[25] The carrier transports have been investigated by many researchers who have demonstrated the potential of core–shell structures. The first experimental evidence of the hole gas accumulation in Ge/Si core–shell NWs was reported in 2005.[11] The enhancement of carrier mobility has, in fact, been shown to be better than that in current types of planar Si MOSFET devices. The formation of crystalline shell layers, however, is a key challenge. Techniques for controlling crystallinity and morphology have been vigorously investigated with the aim of achieving smooth, single-crystal shells on the surfaces of core NWs.[26–33] Stress is induced in Si and Ge heterostructures, which affects the crystallinity of the shell layers. Strain analyses have been used to investigate core–shell NWs by transmission electron microscopy (TEM), Raman, and X-ray diffraction (XRD) measurements.[26–28,33,34] Stress in Si and Ge heterostructures lifts the band-edge degeneracies that affect the transport masses and reduces intervalley or interband scattering.[35,36] Contamination by Au, which is often used as a catalyst for NW growth, needs to be eliminated because Au can diffuse over the surface of core NWs during shell formation.[20,37] These problems need to be overcome to realize high mobility channels using core–shell NWs.

* Address correspondence to fukata.naoki@nims.go.jp.

Received for review August 27, 2015 and accepted November 11, 2015.

Published online 10.1021/acsnano.5b05394

To realize the enhancement of carrier mobility in core−shell NWs, doping sites and the electrical activity of impurity atoms need to be controlled. We have established and reported characterization methods of impurity atoms in SiNWs,[38−41] GeNWs,[42] and their core−shell NWs.[34] Raman scattering is a useful technique for investigating the bonding states and electrical activity of dopant atoms. The former can be clarified by studying the local vibrational modes of impurity atoms, and the latter can be estimated using the Fano effect that appears in optical phonon modes.[38−44] The accumulation of hole gas by forming Ge/Si core−shell NWs has been investigated using this technique of Zhang *et al.*[45] They showed a slight change of the Ge optical phonon peak, and finally concluded that it was due to the Fano effect. The Ge optical phonon peak is also affected by the phonon confinement effect due to the nanoscale size effect and stress due to the heterostructure. In order to completely demonstrate the contribution of the Fano effect, those effects have to be distinguished but were not done in their works.[45] They also formed a Si shell layer at 450 °C and annealed it at 600 °C for 30 min to crystallize the shell.[45] We also performed the same experiments at the same temperature range; however, the shell layer was not completely crystallized, and B activation was not perfect. In a previous paper, we showed the growth of four different types of Si/Ge (i-Si/n-Ge, p-Si/i-Ge) and Ge/Si (n-Ge/i-Si, i-Ge/p-Si) core−shell NWs and demonstrated the selective doping in the core and shell regions, respectively, by means of Raman scattering and XRD measurements.[34] Here, i-Si/n-Ge and p-Si/i-Ge mean intrinsic Si/n-type Ge and p-type Si/intrinsic Ge, respectively. The data clearly showed that boron (B) and phosphorus (P) atoms are electrically activated in the core and shell regions depending on the structure. The optimum p-Si shell formation temperature was 700 °C. The complete dopant activation is also very important to detect the hole accumulation in core−shell NWs.

In this paper, we report our clear verification about the hole gas accumulation from B-doped p-Si shell regions to undoped i-Ge core regions in i-Ge/p-Si core−shell NWs. The p-Si shell was formed at the optimal temperature of 700 °C. We were able to clearly show the electrical activation of B acceptors in the p-Si shell layer and at the same time demonstrate hole accumulation in the i-Ge core region from analysis of the Fano resonance in both Si and Ge optical phonons by Raman scattering measurements. The key point in this analysis is that we successfully disentangled three effects (the phonon confinement effect, the stress effect due to the heterostructures, and the Fano effect) and finally gave a conclusive demonstration of hole gas accumulation in Ge/Si core−shell NWs from the Fano effect and a validation of previous theoretical models.[10,18] The Raman data showed no interdiffusion of B atoms from the p-Si shell to the i-Ge core. In addition to this, high-resolution TEM images of i-Ge/p-Si core−shell NWs showed a very clear interface between the Ge core and the Si shell. Furthermore, we show below that the concentration of hole gas can be roughly controlled by tuning the B-doping concentration in the p-Si shell layers.

RESULTS AND DISCUSSION

Structural characterization of core−shell NWs was performed by TEM, scanning transmission electron microscopy (STEM), and energy-dispersive X-ray (EDX) measurements, as shown in Figure 1. All results clearly show the formation of Ge/Si core−shell NWs. Here, the red and blue parts, respectively, represent the Si and Ge regions in the results of EDX measurements. TEM measurements revealed clear lattice fringes in the core and shell regions. The extremely clear and large high-resolution TEM images we obtained are shown in Figures S1 and S2 in the Supporting Information. They show a clear interface between the Ge core and the Si shell, suggesting no intermixing of Ge and Si at 700 °C. The crystallinity of core−shell NWs is also shown by the results of the XRD and Raman measurements described below. The thickness of the shell layer depends on the shell growth time and the flux of B_2H_6 gas (Figure 1f). The former dependence is as would be expected, while the latter dependence can be explained by the enhancement of radial growth by B_2H_6 gas.[19,34]

The electrical activation of B atoms and the location of hole carriers in core−shell NWs can be determined by Raman measurements using the Fano effect.[34,38,43,44] The representative Raman spectra are shown in Figure 2a,b. The Si optical phonon peak for i-Ge/p-Si (B_2H_6 = 0.5 sccm, 5 min) shows an asymmetric broadening toward higher wavenumbers compared to i-Ge/p-Si (B_2H_6 = 0.1 sccm, 5 min), most likely resulting from the Fano effect.[34,38,43,44] The Fano effect is caused by coupling between discrete optical phonons and the continuum of interband hole excitations in degenerately doped p-type Si. The observation of the Fano effect means that B atoms are electrically activated in the Si shell layers. The asymmetric broadening becomes more pronounced, meaning that the B-doping concentration has increased with increasing B_2H_6 gas flux. The peak observed around 300 cm^{-1} is due to the Ge optical phonon peak. An optical phonon peak related to Si−Ge bonds was also observed, but its intensity was extremely low, suggesting that intermixing of Si and Ge at the interfaces had been suppressed. Figure 2c,d shows the Raman shift of the Si and Ge optical phonon peaks as a function of the shell growth time. The detailed data are also shown in Figure S3 in the Supporting Information. The peak position depends significantly on shell growth time. The downshift of the Si optical phonon peak for the shell growth time of 30 s is mainly due to the tensile stress from the Ge core region. The Si optical

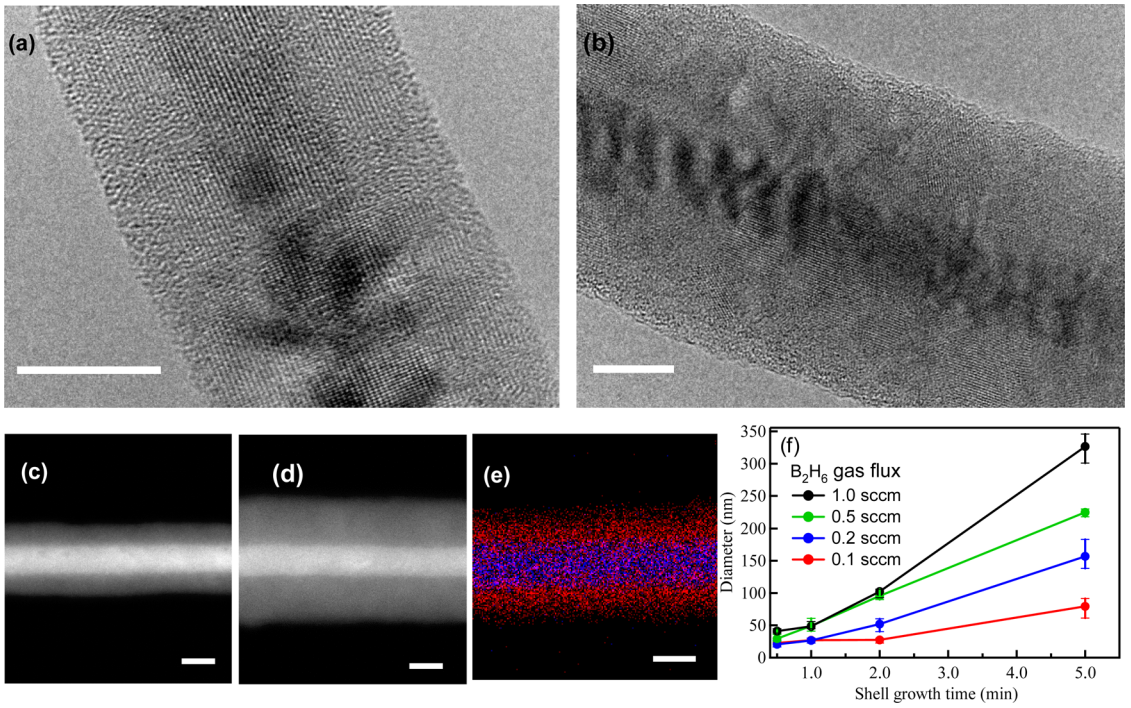

Figure 1. TEM images of i-Ge/p-Si core–shell NWs with shell growth times of (a) 30 s and (b) 1 min. STEM images of i-Ge/p-Si core–shell NWs with shell growth times of (c) 30 s and (d) 1 min. (e) EDX images of i-Ge/p-Si core–shell NWs with a shell growth time of 30 s. (f) B_2H_6 gas flux of p-Si layers was 0.5 sccm. The scale bars are 10 nm. Dependence of the total diameter of core–shell NWs on shell growth time.

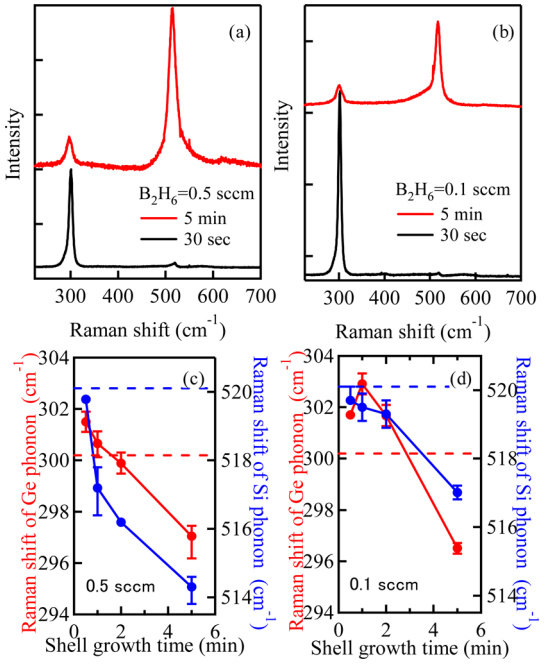

Figure 2. Raman spectra observed for i-Ge/p-Si core–shell NWs. The B_2H_6 gas fluxes of p-Si layers were (a) 0.5 and (b) 0.1 sccm. Raman shift of Si and Ge optical phonon peaks as a function of shell growth time: (c) 0.5 sccm and (d) 0.1 sccm. The red and blue dotted lines show the optical phonon peaks for bulk Ge and bulk Si, respectively.

phonon peak shows a further downshift with increased shell growth time. There are two reasons. First, it can be explained by the Fano effect (doping effect). This means that an increase in the B-doping concentration occurs with an increase of the shell growth time, even though the B_2H_6 gas flux is constant during shell formation. The second reason is due to stress relaxation caused by introducing dislocations in the shell layers. This will be explained in Figure 4 below. The Ge optical phonon peak shows an upshift in short shell growth times, which is due to the compressive stress applied by the Si shell. The Ge optical phonon peak therefore shows a downshift with increased shell growth time. There are two possible explanations for this. The first is hole accumulation due to the formation of core–shell structures. The second is direct B-doping into the i-Ge core by the interdiffusion of B atoms from the Si shell during shell formation. However, the second possibility can be rejected. More conclusive proof is shown in the results and discussion below.

The results of XRD measurements also support the possibility of hole accumulation. Figure 3a shows the representative Ge(111) and Si(111) XRD peaks observed for i-Ge/p-Si (0.1 sccm). The results of i-Ge/p-Si (0.5 sccm) are shown in Figures S4 and S5. The Ge(111) peak shifts to a lower angle, while the Si(111) peak shifts to a higher angle with increased shell growth time. To make the dependence clearer, the average lattice constants of Ge and Si in the core–shell NWs were calculated by fitting the Ge- and the Si-related XRD peaks. The average lattice constant of the Si shell is greater than that for bulk Si, as shown in Figure 3c, which is due to the tensile stress from the Ge core.

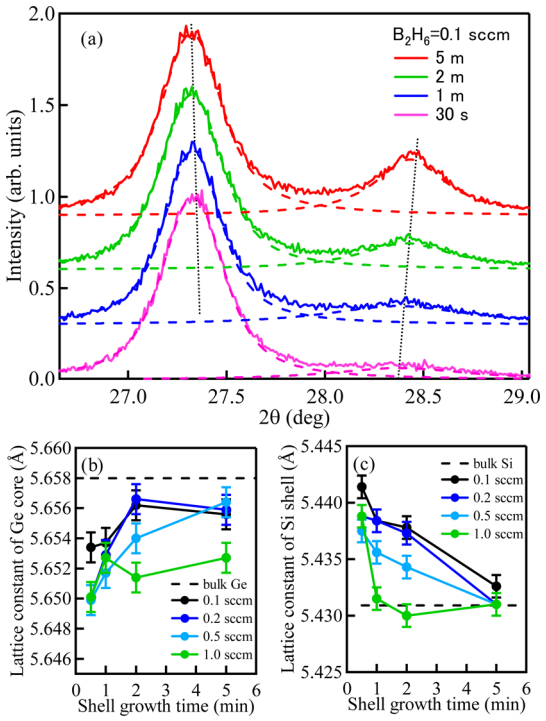

Figure 3. (a) XRD spectra of Ge(111) and Si(111) peaks observed for i-Ge/p-Si core−shell NWs. The dotted lines in (a) are deconvoluted peaks by fitting. The lattice constant of the (b) Ge core and (c) Si shell in the i-Ge/p-Si core−shell NWs. The results show the dependence on the shell growth time. The dotted lines show the lattice constants of bulk Ge and bulk Si.

The Si lattice constant decreased with increased shell growth time, showing that tensile stress is attenuated by increasing the Si shell thickness (Figure 3c). One of the reasons is stress relaxation due to the formation of thicker shell layers and the effects of longer annealing. As shown in Figures 4a,b, the Si shell layer clearly changed from the single-crystal-type to the polycrystalline-type with an increased Si shell layer thickness, resulting in stress relaxation (Figure 4c). The lattice contraction caused by the doping of B atoms with diameters smaller than those of Si is also one possible reason because the increase in shell growth time increases the B-doping concentration in the Si shell.[34] On the other hand, the average lattice constant of the Ge shell is smaller than that for bulk Ge, which is due to the compressive stress applied by the Si shell. It was weakened with increased shell growth time due to the relaxation of the thick Si layers. The increase in the Ge lattice constant with an increase of the shell growth time is more likely to eliminate the risk of interdiffusion of B atoms into the Ge core during shell formation because introducing B atoms causes lattice contraction of the Ge core. This can be explained as follows. In our previous paper about impurity doping in GeNWs,[42] we observed an upshift of the Ge(111) peak by XRD and the Fano effect in the Ge optical phonon peak by Raman spectroscopy. The former XRD peak shift is due to the lattice contraction in GeNWs by high

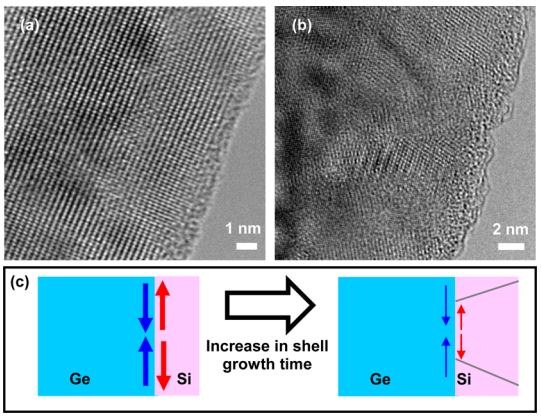

Figure 4. High-resolution TEM images of i-Ge/p-Si (0.5 sccm) core−shell NWs with Si shell growth times of (a) 30 s and (b) 1 min. (c) Schematic illustrations of crystallinity and stress in i-Ge/p-Si (0.5 sccm) core−shell NWs as a function of the Si shell growth time.

concentration B-doping, while the latter Fano effect is due to the existence of a high concentration of hole carriers in GeNWs. The results clearly show that high concentration B-doping in the Ge region gives the XRD peak shift and the Fano effect at the same time. In this work, we could detect the Fano effect in the Ge optical phonon peak, while the upshift of the XRD peak was not observed. If the Fano effect is due to the B atoms introduced from the p-Si shell layers, the B concentration should be higher than 10^{17} cm^{-3}; finally, the Ge(111) XRD peak should show the upshift. However, we did not observe it. Hence, the XRD data provide additional evidence that the downshift of the Ge optical phonon peak is due to the accumulation of hole gas on forming core−shell structures.

To further demonstrate the hole accumulation into the i-Ge core in i-Ge/p-Si core−shell NWs, we summarized the Raman data as a function of the B_2H_6 gas flux in Figure 5. The downshift and asymmetric broadening of the Si optical phonon peak, which is due to the Fano effect, become more pronounced with increased B_2H_6 gas flux, showing the increase in the B-doping concentration in the Si shell layers (Figure 5b,e). The Ge optical phonon peak also clearly shows the downshift and asymmetric broadening with increased B_2H_6 gas flux for the formation of the p-Si shell layers (Figure 5a, c,d). This downshift and asymmetric broadening are explained below. Figure 5c shows a comparison of the Ge optical phonon peaks observed for i-Ge/p-Si (1.0 sccm) core−shell NWs, i-Ge/i-Si (0 sccm) core−shell NWs, i-GeNWs, and bulk Ge. The Ge optical phonon peak for i-GeNWs shows a slight downshift and asymmetric broadening compared to bulk Ge. This is due to the phonon confinement effect because the diameter of GeNWs is about 10 nm.[42,46−48] The Ge optical phonon peak shows an upshift and asymmetric broadening due to the formation of i-Si shell layers (light blue spectrum). This upshift can be explained by the compressive stress applied by the i-Si shell layers,

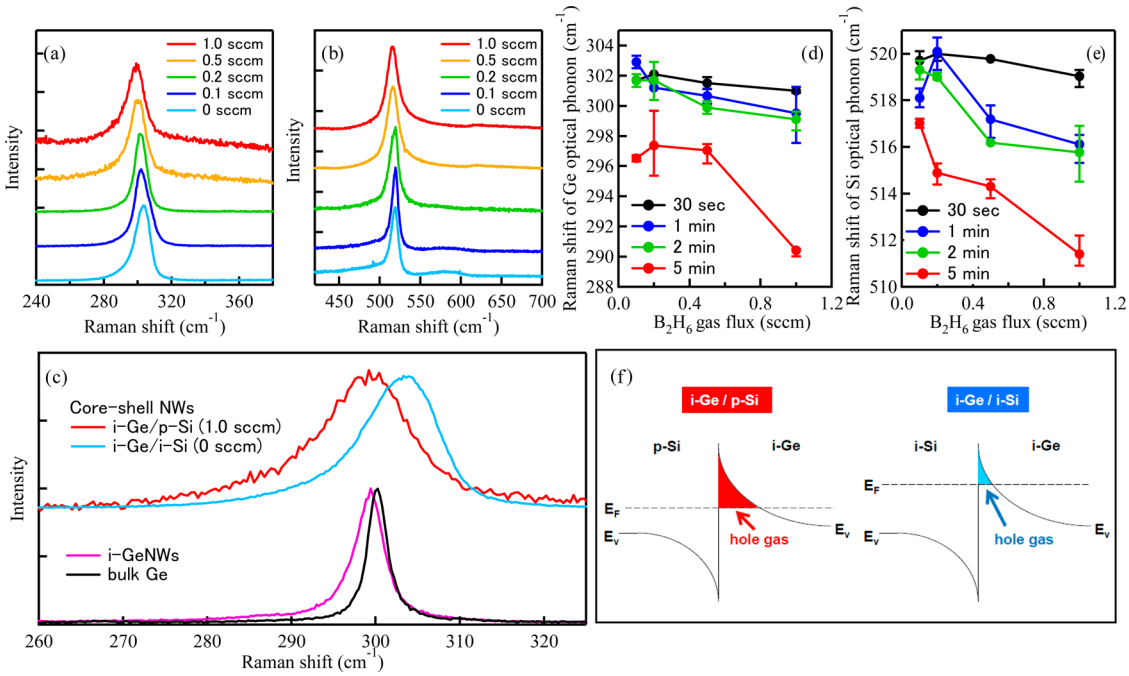

Figure 5. (a) Ge and (b) Si optical phonon peak observed for i-Ge/p-Si core–shell NWs. (c) Comparison of the Ge optical phonon peaks observed for i-Ge/p-Si (1.0 sccm) core–shell NWs, i-Ge/i-Si (0 sccm) core–shell NWs, i-GeNWs, and bulk Ge. The B_2H_6 gas fluxes of p-Si layers were changed from 0 to 1.0 sccm. The shell growth time is 2 min. Raman shift of the (d) Ge and (e) Si optical phonon peaks as a function of the B_2H_6 gas flux. The red and blue dotted lines show the optical phonon peaks for bulk Si and bulk Ge, respectively. (f) Band diagram around a Si–Ge heterojunction in Ge/Si core–shell NWs. E_v and E_f are the valence band edge and the Fermi energy, respectively.

whereas the asymmetric broadening cannot be explained by compressive stress alone: it suggests the effect of hole accumulation. The Ge optical phonon peak showed a downshift and further asymmetric broadening with increased B concentration in the Si shell layers, as shown in the red spectrum of the i-Ge/p-Si (1.0 sccm) core–shell NWs. This can be explained in mostly by the Fano effect, showing the introduction of a high concentration of holes in the i-Ge core region. The result clearly demonstrates hole accumulation from the p-Si (i-Si) shell to the i-Ge core region that results from the formation of core–shell NW structures. We also performed HF etching experiments (see section 4 in Supporting Information). The asymmetric broadening of the Ge optical phonon peak was decreased, and the peak shifted to higher wavenumbers after HF etching, as shown in Figure S6. The thickness of B-doped Si shell layers decreases as a result of HF etching, and the number of holes introduced into the Ge core region is likely to be reduced, resulting in a decrease in hole accumulation in the Ge core region. This result also supports hole accumulation due to the formation of core–shell NW structures. As shown in Figure 5f, there is an abrupt band discontinuity between Si and Ge, which is called the band offset. The energy band diagram was illustrated by reference to the previous reports.[10,18,45] To maintain a constant chemical potential throughout the two materials of Si and Ge, holes flow from the p-Si (i-Si) to the i-Ge region. This causes the band edges to bend at the interface,

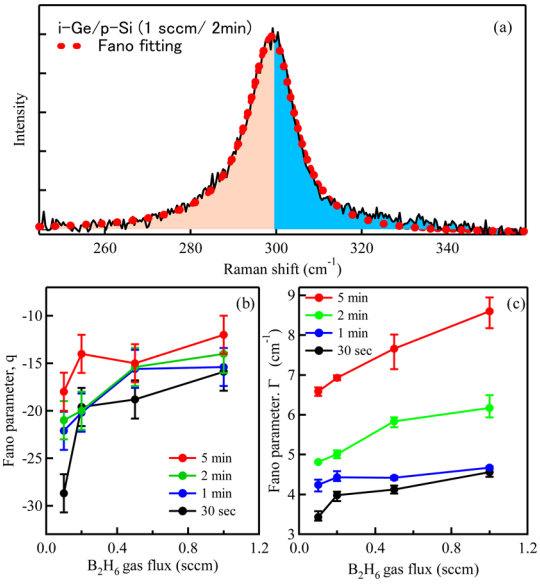

Figure 6. Ge optical phonon peak observed for i-Ge/p-Si core–shell NWs (1 sccm, 2 min). The red dotted line shows fitting data using the Fano equation. Fano parameters of (b) q and (c) Γ estimated from the Ge optical phonon peaks observed for i-Ge/p-Si core–shell NWs.

with the result that holes are confined in the i-Ge region as hole gas. The Fermi level is shifted from the middle of the band gap to the acceptor level with an increase in B concentration in the p-Si layer. This increases the hole gas density in the i-Ge region. Hence, our data clearly demonstrate hole accumulation

due to the formation of i-Ge/p-Si core−shell NW structures and show the validity of previous theoretical models.[10,18]

The hole accumulation in the Ge core region increased with increasing B concentration in the Si shell layers in the i-Ge/p-Si core−shell NWs, meaning that the hole gas density in the Ge core can be controlled by shell doping. We analyzed the Ge optical phonon peaks using the Fano equation.[43] The asymmetric line shape of the optical phonon due to the Fano effect is given by

$$I(\omega) = I_0 \frac{(q+\varepsilon)^2}{(1+\varepsilon^2)} \quad (1)$$

where ω is the wavenumber, I_0 the prefactor, q the asymmetry parameter; ε is given by $\varepsilon = (\omega-\omega_p)/\Gamma$, where ω_p is the phonon wavenumber and Γ is the line width parameter. One of the fitting results is shown in Figure 6a. The two important values of q and Γ are summarized in Figure 6b,c. These two values increased with increased B_2H_6 gas flux. This is due to the increase in the hole accumulation in the Ge core region. Generally, hole density can be roughly estimated according to the Fano parameters. However, the two effects—the stress induced by the heterostructures and the phonon confinement effect caused by the nanoscale sizes—make it difficult to estimate the exact hole density in the Ge shell. If we ignore these two effects, the hole density in the Ge shell is estimated to be $10^{17}-10^{18}$ cm^{-3}.

CONCLUSION

A precise analysis of the Ge optical phonon peak by Raman spectroscopy was able to disentangle three effects, the phonon confinement effect, the stress effect due to the heterostructures, and the Fano effect, ultimately providing a clear demonstration of hole gas accumulation in i-Ge/p-Si core−shell NWs. The results of XRD measurements also support the Raman data. These results show the realization of one type of high electron mobility transistor structure in one-dimensional NWs. The concentration of hole gas was controlled by the B-doping concentration in the Si shell.

EXPERIMENTAL METHODS

i-Ge/p-Si core−shell nanowires were grown on a Si(111) substrate by chemical vapor deposition with a background pressure of 2×10^{-6} Pa. The low background pressure makes it possible to obtain a clear interface between Si and Ge without oxidation. Gold nanocolloid particles were used as seeds for vapor−liquid−solid growth[49] of core GeNWs using 10 sccm of GeH_4 (100%). The total pressure was set at 8 Torr by mixing with N_2 gas. The axial growth of i-GeNWs was performed at 320 °C for 30 min, and the subsequent radial growth of the p-Si shell layer was achieved at 700 °C using 19 sccm of SiH_4 (100%) and 0−5 sccm of B_2H_6 (1% in H_2) to form the i-Ge/p-Si core−shell NWs. Doping with B was performed during the vapor−solid growth of the Si shell layer in the i-Ge/p-Si core−shell NWs. These growth conditions were determined to be able to prevent the interdiffusion of B into Ge and the intermixing of Si−Ge. A detailed explanation is reported in ref 34.

Micro-Raman scattering measurements were performed at room temperature using a 100× objective and a 532 nm excitation light source with an excitation power of approximately 0.02 mW to prevent local heating effects by the excitation laser.[46,50] The spectral resolution of all data was about 0.3 cm^{-1}. These measurements clarify the states of B atoms and stress in core−shell NWs and finally demonstrate B-doping in the p-Si shell regions and hole accumulation in the i-Ge core regions. X-ray diffraction measurements were also performed to investigate individually the stress in the core and shell regions. The XRD data were collected with parallel beam geometry using Cu Kα radiation. The structures of core−shell NWs were investigated by field emission scanning electron microscopy, STEM, TEM, and EDX analysis. The EDX measurements were performed during the TEM measurements.

Conflict of Interest: The authors declare no competing financial interest.

Supporting Information Available: The Supporting Information is available free of charge on the ACS Publications website at DOI: 10.1021/acsnano.5b05394.

Additional information and figures (PDF)

Acknowledgment. This work was supported by JSPS Kakenhi (No. 26246021) and the World Premier International Research Center Initiative (WPI Initiative), MEXT, Japan.

REFERENCES AND NOTES

1. Li, Y.; Qian, F.; Lieber, C. M. Nanowire Electronic and Optoelectronic Devices. *Mater. Today* **2006**, *9*, 18–27.
2. Thelander, C.; Agarwal, P.; Brongersma, S.; Eymery, J.; Feiner, L. F.; Forchel, A.; Scheffler, M.; Riess, W.; Ohlsson, B. J.; Gösele, U.; Samuelson, L. Nanowire-Based One-Dimensional Electronics. *Mater. Today* **2006**, *9*, 28–35.
3. Pauzauskie, P. J.; Yang, P. Nanowire Photonics. *Mater. Today* **2006**, *9*, 36–45.
4. Ma, D. D. D.; Lee, C. S.; Au, A. C. K.; Tong, S. Y.; Lee, S. T. Small Diameter Silicon Nanowire Surface. *Science* **2003**, *299*, 1874–1877.
5. Fan, H. J.; Werner, P.; Zacharias, M. Semiconductor Nanowires: From Self-Organization to Patterned Growth. *Small* **2006**, *2*, 700–717.
6. Wang, Z. L.; Song, J. Piezoelectric Nanogenerators Based on Zinc Oxide Nanowire Arrays. *Science* **2006**, *312*, 242–246.
7. Chockla, A. M.; Korgel, B. A. Seeded Germanium Nanowire Synthesis in Solution. *J. Mater. Chem.* **2009**, *19*, 996–1001.
8. Perea, D. E.; Hemesath, E. R.; Schwalbach, E. J.; Lensch-Falk, J. L.; Voorhees, P. W.; Lauhon, L. J. Direct Measurement of Dopant Distribution in an Individual Vapour-Liquid-Solid Nanowire. *Nat. Nanotechnol.* **2009**, *4*, 315–319.
9. Bierman, M. J.; Lau, Y. K. A.; Kvit, A. V.; Schmitt, A. L.; Jin, S. Dislocation-Driven Nanowire Growth and Eshelby Twist. *Science* **2008**, *320*, 1060–1063.
10. Lauhon, L. J.; Gudiksen, M. S.; Wang, D.; Lieber, C. M. Core-Multishell Nanowire Heterostructures. *Nature* **2002**, *420*, 57–61.
11. Lu, W.; Xiang, J.; Timko, B. P.; Wu, Y.; Lieber, C. M. One-Dimensional Hole Gas in Germanium/Silicon Nanowire Heterostructures. *Proc. Natl. Acad. Sci. U. S. A.* **2005**, *102*, 10046–10051.
12. Musin, R. N.; Wang, X. Q. Structural and Electronic Properties of Epitaxial Core-Shell Nanowire Heterostructures. *Phys. Rev. B: Condens. Matter Mater. Phys.* **2005**, *71*, 155318.
13. Xiang, J.; Lu, W.; Hu, Y.; Wu, Y.; Yan, H.; Lieber, C. M. Ge/Si Nanowire Heterostructures as High-Performance Field-Effect Transistors. *Nature* **2006**, *441*, 489–493.
14. Liang, G.; Xiang, J.; Kharche, N.; Klimeck, G.; Lieber, C. M.; Lundstrom, M. Performance Analysis of a Ge/Si Core/Shell

Nanowire Field-Effect Transistor. *Nano Lett.* **2007**, *7*, 642–646.
15. Hu, Y.; Xiang, J.; Liang, G.; Yan, H.; Lieber, C. M. Sub-100 Nanometer Channel Length Ge/Si Nanowire Transistors with Potential for 2 THz Switching Speed. *Nano Lett.* **2008**, *8*, 925–930.
16. Park, J.-S.; Ryu, B.; Moon, C.-Y.; Chang, K. J. Defects Responsible for the Hole Gas in Ge/Si Core-Shell Nanowires. *Nano Lett.* **2010**, *10*, 116–121.
17. Li, L.; Smith, D. J.; Dailey, E.; Madras, P.; Drucker, J.; Mccartney, M. R. Observation of Hole Accumulation in Ge/Si Core/Shell Nanowires Using off-Axis Electron Holography. *Nano Lett.* **2011**, *11*, 493–497.
18. Amato, M.; Ossicini, S.; Rurali, R. Band-Offset Driven Efficiency of the Doping of SiGe Core-Shell Nanowires. *Nano Lett.* **2011**, *11*, 594–598.
19. Zhao, Y.; Smith, J. T.; Appenzeller, J.; Yang, C. Transport Modulation in Ge/Si Core/Shell Nanowires through Controlled Synthesis of Doped Si Shells. *Nano Lett.* **2011**, *11*, 1406–1411.
20. Dayeh, S. A.; Gin, A. V.; Picraux, S. T. Advanced Core/Multishell Germanium/Silicon Nanowire Heterostructures: Morphology and transport. *Appl. Phys. Lett.* **2011**, *98*, 163112.
21. Amato, M.; Palummo; Ossicini, S. Band Structure Analysis in SiGe Nanowires. *Mater. Sci. Eng., B* **2012**, *177*, 705–711.
22. Amato, M.; Palummo, M.; Rurali, R.; Ossicini, S. Optical Absorption Modulation by Selective Codoping of SiGe Core-Shell Nanowires. *J. Appl. Phys.* **2012**, *112*, 114323.
23. Nguyen, B.-M.; Taur, Y.; Picraux, S. T.; Dayeh, S. A. Diameter-Independent Hole Mobility in Ge/Si Core/Shell Nanowire Field Effect Transistors. *Nano Lett.* **2014**, *14*, 585–591.
24. Amato, M.; Palummo, M.; Rurali, R.; Ossicini, S. Silicon–Germanium Nanowires: Chemistry and Physics in Play, from Basic Principles to Advanced Applications. *Chem. Rev.* **2014**, *114*, 1371–1412.
25. Mimura, T.; Hiyamizu, S.; Fujii, T.; Nanbu, K. A New Field-Effect Transistor with Selectively-Doped GaAs/AlGaAs Heterojunctions. *Jpn. J. Appl. Phys.* **1980**, *19*, L225–L227.
26. Pan, L.; Lew, K. K.; Redwing, J. M.; Dickey, E. C. Stranski-Krastanow Growth of Germanium on Silicon Nanowires. *Nano Lett.* **2005**, *5*, 1081–1085.
27. Goldthorpe, I. A.; Marshall, A. F.; McIntyre, P. C. Synthesis and Strain Relaxation of Ge-Core/Si-Shell Nanowire arrays. *Nano Lett.* **2008**, *8*, 4081–4086.
28. Goldthorpe, I. A.; Marshall, A. F.; McIntyre, P. C. Inhiiting Strain-Induced Surface Roughening: Dislocation-Free Ge/Si and Ge/SiGe Core-Shell Nanowires. *Nano Lett.* **2009**, *9*, 3715–3719.
29. Swadener, J. G.; Picraux, S. T. Strain Distributions and Electronic Property Modifications in Si/Ge Axial Nanowire Heterostructures. *J. Appl. Phys.* **2009**, *105*, 044310.
30. Ben-Ishai, M.; Patolsky, F. A Route to High-Quality Crystalline Coaxial Core/Multishell Ge@Si(GeSi)$_n$ and Si@(GeSi)$_n$ Nanowire Heterostructures. *Adv. Mater.* **2010**, *22*, 902–906.
31. Dayeh, S. A.; Wang, J.; Li, N.; Huang, J. Y.; Gin, A. V.; Picraux, S. T. Growth, Defect Formation, and Morphology Control of Germanium_Silicon Semiconductor Nanowire Heterostructures. *Nano Lett.* **2011**, *11*, 4200–4206.
32. Hu, S.; Kawamura, Y.; Huang, K. C. Y.; Li, Y.; Marshall, A. F.; Itoh, K. M.; Brongersma, M. L.; McIntyre, P. C. Thermal Stability and Surface Passivation of Ge Nanowires Coated by Epitaxial SiGe Shells. *Nano Lett.* **2012**, *12*, 1385–1391.
33. Dayeh, S. A.; Tang, W.; Boioli, F.; Kavanagh, K. L.; Zheng, H.; Wang, J.; Mack, N. H.; Swadener, G.; Huang, J. Y.; Miglio, L.; Tu, K.-N.; Picraux, S. T. Direct Measurement of Coherency Limits for Strain Relaxation in Heteroepitaxial Core/Shell Nanowires. *Nano Lett.* **2013**, *13*, 1869–1876.
34. Fukata, N.; Mitome, M.; Sekiguchi, T.; Bando, Y.; Kirkham, M.; Hong, J.-I.; Wang, Z. L.; Snyder, R. Characterization of Impurity Doping and Stress in Si/Ge and Ge/Si Core–Shell Nanowires. *ACS Nano* **2012**, *6*, 8887–8895.
35. Oberhuber, R.; Zandler, G.; Vogl, P. Subband Structure and Mobility of Two-Dimensional Holes in Strained Si/SiGe MOSFET's. *Phys. Rev. B: Condens. Matter Mater. Phys.* **1998**, *58*, 9941–9948.
36. Fischetti, M. V.; Ren, Z.; Solomon, P. M.; Yang, M.; Rim, K. Six-Band k-p Calculation of the Hole Mobility in Silicon Inversion layers: Dependence on Surface Orientation, Strain, and Silicon Thickness. *J. Appl. Phys.* **2003**, *94*, 1079–1095.
37. Dayeh, S. A.; Mack, N. H.; Huang, J. Y.; Picraux, S. T. Advanced Core/Shell Germanium/Silicon Nanowire Heterostructures: The Au-Diffusion Bottleneck. *Appl. Phys. Lett.* **2011**, *99*, 023102.
38. Fukata, N.; Chen, J.; Sekiguchi, T.; Okada, N.; Murakami, K.; Tsurui, T.; Ito, S. Doping and Hydrogen Passivation of B in Silicon Nanowires Synthesized by Laser Ablation. *Appl. Phys. Lett.* **2006**, *89*, 203109.
39. Fukata, N.; Chen, J.; Sekiguchi, T.; Matsushita, S.; Oshima, T.; Uchida, N.; Murakami, K.; Tsurui, T.; Ito, S. Phosphorus Doping and Hydrogen Passivation of Donors and Defects in Silicon Nanowires Synthesized by Laser Ablation. *Appl. Phys. Lett.* **2007**, *90*, 153117.
40. Fukata, N. Impurity Doping in Silicon Nanowires. *Adv. Mater.* **2009**, *21*, 2829–2832.
41. Fukata, N. Doping and Characterization of Impurity Atoms in Si and Ge Nanowires. *phys. status solidi C* **2014**, *11*, 320–330.
42. Fukata, N.; Sato, K.; Mitome, M.; Bando, Y.; Sekiguchi, T.; Kirkham, M.; Hong, J. I.; Wang, Z. L.; Snyder, R. L. Doping and Raman Characterization of Boron and Phosphorus Atoms in Germanium Nanowires. *ACS Nano* **2010**, *4*, 3807–3816.
43. Fano, U. Effects of Configuration Interaction on Intensities and Phase Shifts. *Phys. Rev.* **1961**, *124*, 1866–1878.
44. Olego, D.; Cardona, M. Self-Energy Effects of the Optical Phonons of Heavily Doped p-GaAs and p-Ge. *Phys. Rev. B: Condens. Matter Mater. Phys.* **1981**, *23*, 6592–6602.
45. Zhang, S.; Lopez, F. J.; Hyun, J. K.; Lauhon, L. J. Direct Detection of Hole Gas in Ge-Si Core-Shell Nanowires by Enhanced Raman Scattering. *Nano Lett.* **2010**, *10*, 4483–4487.
46. Fukata, N.; Oshima, T.; Murakami, K.; Kizuka, T.; Tsurui, T.; Ito, S. Phonon Confinement effect of Silicon Nanowires Synthesized by Laser Ablation. *Appl. Phys. Lett.* **2005**, *86*, 213112.
47. Richter, H.; Wang, Z. P.; Ley, L. The One Phonon Raman Spectrum in Microcrystalline Silicon. *Solid State Commun.* **1981**, *39*, 625.
48. Campbell, I. H.; Fauchet, P. M. The Effects of Microcrystal Size and Shape on the One Phonon Raman Spectra of Crystalline Semiconductors. *Solid State Commun.* **1986**, *58*, 739.
49. Wagner, R. S.; Ellis, W. C. VAPOR-LIQUID-SOLID MECHANISM OF SINGLE CRYSTAL GROWTH. *Appl. Phys. Lett.* **1964**, *4*, 89–90.
50. Piscanec, S.; Cantoro, M.; Ferrari, A. C.; Zapien, J. A.; Lifshitz, Y.; Lee, S. T.; Hofmann, S.; Robertson, J. Raman Spectroscopy of Silicon Nanowires. *Phys. Rev. B: Condens. Matter Mater. Phys.* **2003**, *68*, 241312(R).